Baseline Predictions for Electrons From Heavy Flavor Decays and Drell-Yan Production at RHIC II

R. Vogt

Nuclear Science Division, Lawrence Berkeley National Laboratory, Berkeley, CA 94720, USA

Physics Department, University of California, Davis, CA 95616, USA

Outline

- Open Heavy Flavor Production and Decay at RHIC
- Drell-Yan Production at RHIC

Open Heavy Flavor Decays to Leptons

FONLL Calculation of p_T Dependence (Cacciari and Nason)

Designed to cure large logs of p_T/m for $p_T \gg m$ in fixed order calculation (FO) where mass is no longer only relevant scale

Includes resummed terms (RS) of order $\alpha_s^2(\alpha_s \log(p_T/m))^k$ (leading log – LL) and $\alpha_s^3(\alpha_s \log(p_T/m))^k$ (NLL) while subtracting off fixed order terms retaining only the logarithmic mass dependence (the "massless" limit of fixed order (FOM0)), both calculated in the same renormalization scheme

There needs to be a scheme change in the FO calculation since it treats the heavy flavor as heavy while the RS approach includes the heavy flavor as an active light degree of freedom

Schematically then:

$$\text{FONLL} = \text{FO} + (\text{RS} - \text{FOM0})G(m, p_T)$$

The function $G(m, p_T)$ is arbitrary but must approach unity as $m/p_T \to 0$ up to terms suppressed by powers of m/p_T

Total cross section similar to but slightly higher than NLO

One drawback: problems with matching arise at larger rapidity, therefore we don't calculate results for $|y| > 2$

Comparison of FONLL and NLO p_T Distributions

FONLL result for bare charm is slightly higher over most of the p_T range – fixed order result gets higher at large p_T due to large $\log(p_T/m)$ terms

New fragmentation functions (dashed curve) for D^0 harder than Peterson function (dot-dot-dot-dashed curve)

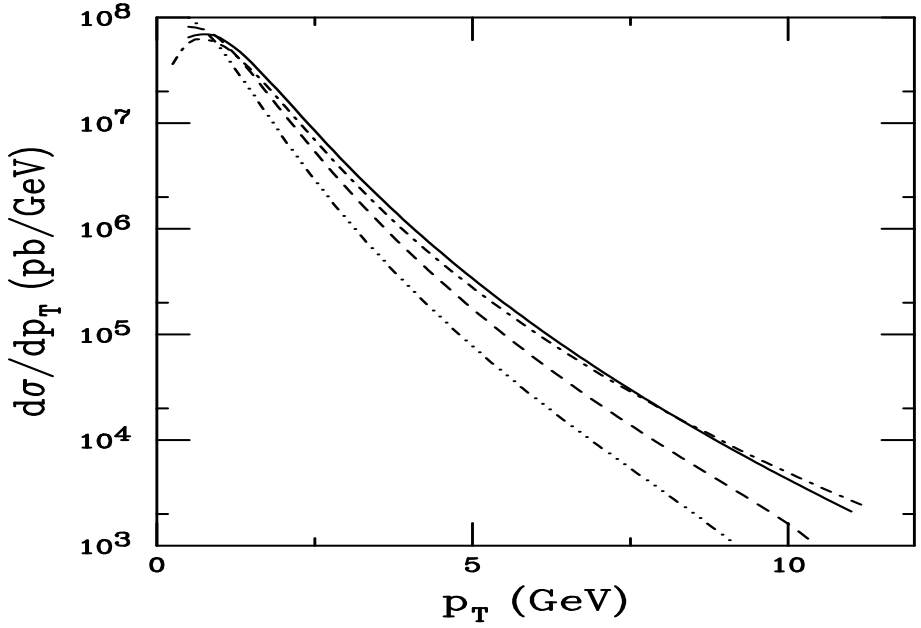

Figure 1: The p_T distributions calculated using FONLL are compared to NLO. The dot-dashed curve is the NLO charm quark p_T distribution. The solid, dashed and dot-dot-dot-dashed curves are FONLL results for the charm quark and D^0 meson with the updated fragmentation function and the Peterson function, respectively. All the calculations are done with the CTEQ6M parton densities, $m = 1.2$ GeV and $\mu = m_T$ in the region $|y| \leq 0.75$.

Uncertainty Bands for p_T Distributions

As we saw for the total cross sections, depending on μ_R, μ_F and m, the maximum and minimum values of the calculated total cross section may come from different curves

Same is true for p_T distributions: upper and lower curves in the band do not represent a single set of μ_R, μ_F and m values but are the upper and lower limits of mass and scale uncertainties added in quadrature:

$$(d\sigma/dp_T)_{\rm max} = (d\sigma/dp_T)_{\rm central} + \sqrt{((d\sigma/dp_T)_{\mu,\rm max} - (d\sigma/dp_T)_{\rm central})^2 + ((d\sigma/dp_T)_{m,\rm max} - (d\sigma/dp_T)_{\rm central})^2}$$
$$(d\sigma/dp_T)_{\rm min} = (d\sigma/dp_T)_{\rm central} - \sqrt{((d\sigma/dp_T)_{\mu,\rm min} - (d\sigma/dp_T)_{\rm central})^2 + ((d\sigma/dp_T)_{m,\rm min} - (d\sigma/dp_T)_{\rm central})^2}$$

The central value is $m = 1.5$ GeV, $\mu_F = \mu_R = m_T$ (using scale m_T rather than m for p_T distributions)

We follow the same procedure for both the NLO and FONLL calculations and compare them in the central ($|y| \leq 0.75$) and forward ($1.2 < y < 2.2$ – $1.2 < y < 2$ for FONLL) regions

Previous results with $m = 1.2$ GeV, $\mu_F = \mu_R = 2m_T$ fall within the uncertainty band

We give results for bare heavy flavors and heavy flavor mesons in pp collisions at $\sqrt{s} = 200$ and 500 GeV

Note that, due to the scale change from m to m_T in the p_T distributions leads to much lower integrated total cross sections for $(\mu_F/m_T, \mu_R/m_T) = (1, 0.5)$ and (0.5,0.5) since $\alpha_s(m_T)$ decreases with p_T

Components of Uncertainty Band at NLO

Curves with $(\mu_F/m_T, \mu_R/m_T) = (1, 0.5)$ and (0.5,0.5) make up the upper scale uncertainty while those with (0.5,1) and (2,2) make up the lower

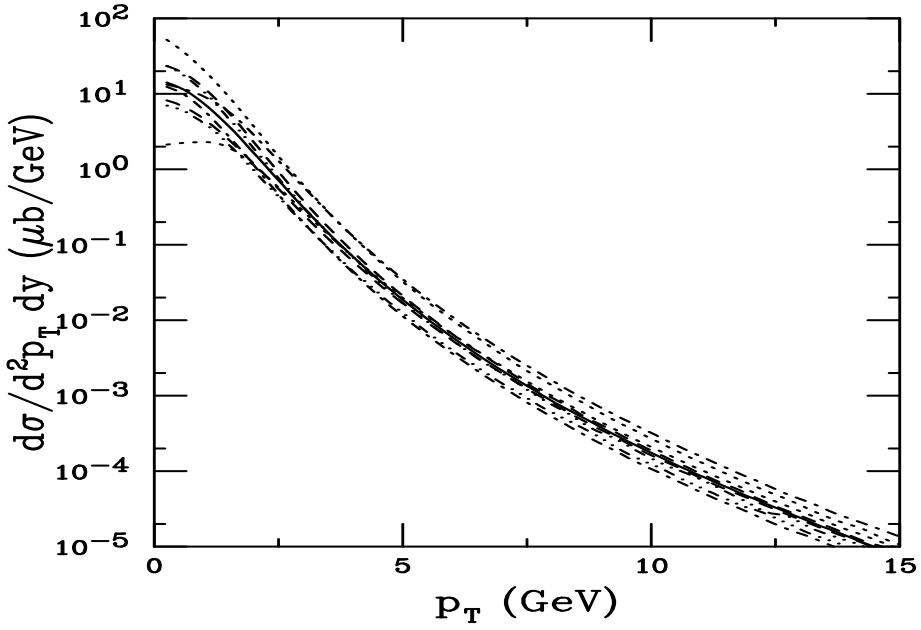

Figure 2: The charm quark p_T distributions calculated using CTEQ6M. The solid curve is the central value $(\mu_F/m_T, \mu_R/m_T) = (1, 1)$ with $m = 1.5$ GeV. The upper and lower dashed curves are $m = 1.3$ and 1.7 GeV with (1,1) respectively. The upper and lower dot-dashed curves correspond to (0.5,0.5) and (2,2) while the upper and lower dotted curves are with (1,0.5) and (0.5,1) and the upper and lower dot-dot-dot-dashed curves are with (2,1) and (1,2) with $m = 1.5$ GeV.

Uncertainty Bands for c and D at 200 GeV

NLO and FONLL bands almost indistinguishable from each other

D meson band uses primary D distributions, not distinguishing charged from neutral D mesons, not possible to separate c and D bands for $p_T < 10$ GeV

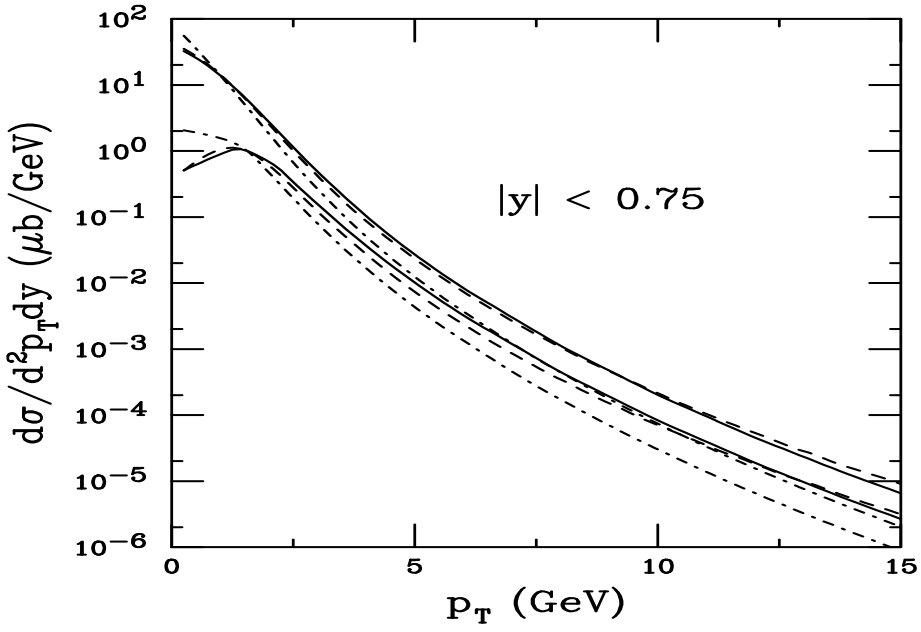

Figure 3: The charm quark theoretical band as a function of p_T for FONLL (solid curves) and NLO (dashed curves) in $\sqrt{s} = 200$ GeV pp collisions in the region $|y| \leq 0.75$. We also show the D meson uncertainty band.

Uncertainty Bands for c and D at 500 GeV

c and D distributions are harder at 500 GeV

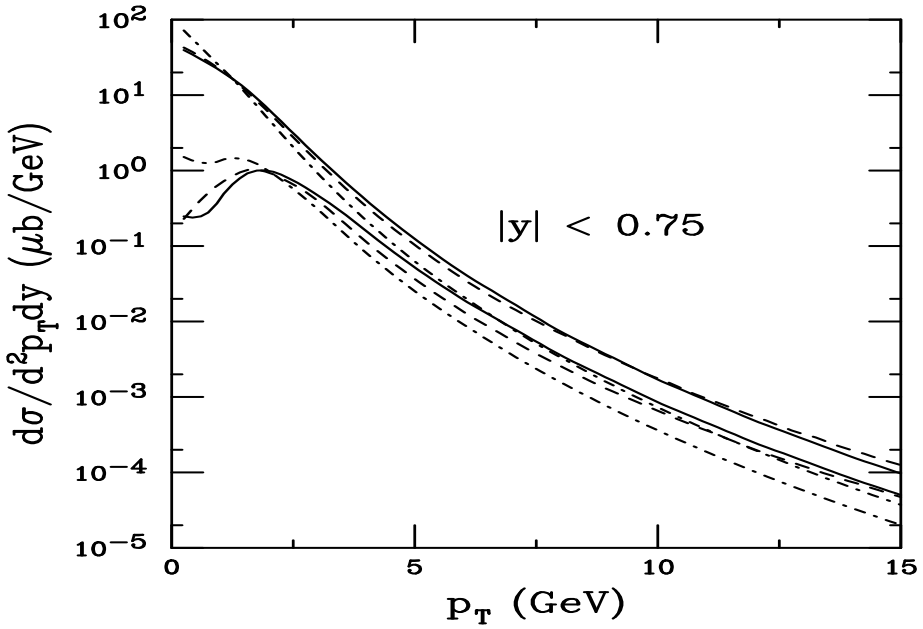

Figure 4: The charm quark theoretical band as a function of p_T for FONLL (solid curves) and NLO (dashed curves) in $\sqrt{s} = 200$ GeV pp collisions in the region $|y| \leq 0.75$. We also show the D meson uncertainty band.

Uncertainty Bands for b and B at 200 GeV

Bands narrower for bottom than for charm and impossible to separate b from B over the p_T range shown (B is a generic B meson)

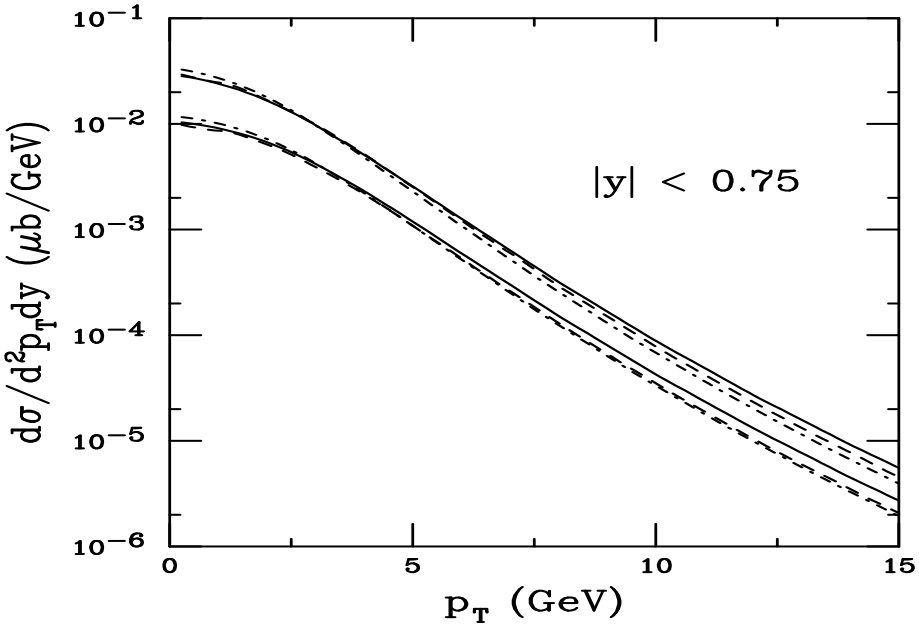

Figure 5: The bottom quark theoretical band as a function of p_T for FONLL (solid curves) and NLO (dashed curves) in $\sqrt{s} = 200$ GeV pp collisions in the region $|y| \leq 0.75$. We also show the B meson uncertainty band.

Uncertainty Bands for b and B at 500 GeV

Much stronger energy dependence and more hardening for bottom than for charm with increasing energy

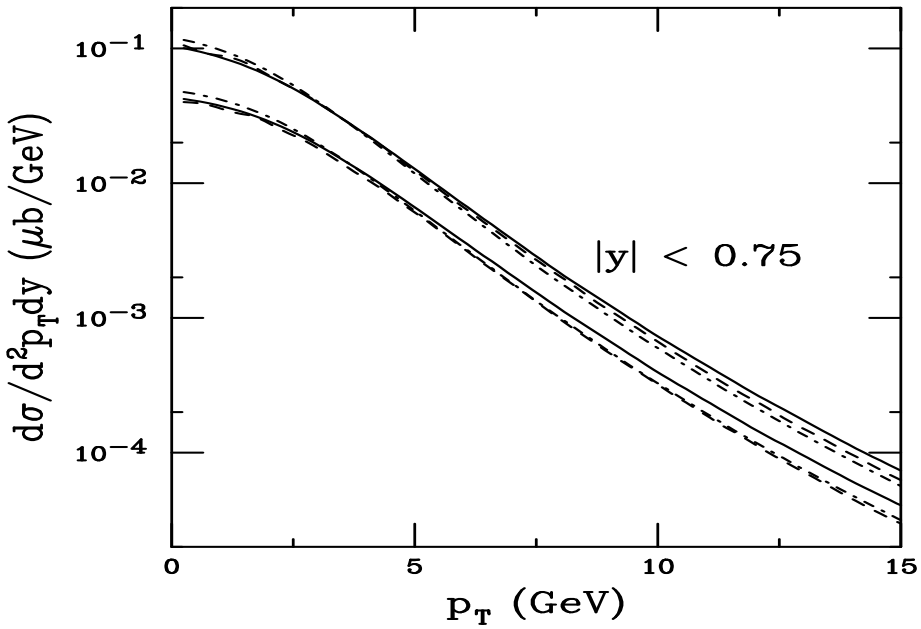

Figure 6: The bottom quark theoretical band as a function of p_T for FONLL (solid curves) and NLO (dashed curves) in $\sqrt{s} = 200$ GeV pp collisions in the region $|y| \leq 0.75$. We also show the B meson uncertainty band.

Obtaining the Electron Spectra From Heavy Flavor Decays

D and B decays to leptons depends on measured decay spectra and branching ratios

$D \to e$ Use preliminary CLEO data on inclusive electrons from semi-leptonic D decays, assume it to be indentical for all charm hadrons

$B \to e$ Primary B decays to electrons measured by Babar and CLEO, fit data and assume fit to work for all bottom hadrons

$B \to D \to e$ Obtain electron spectrum from convolution of $D \to e$ spectrum with parton model calculation of $b \to c$ decay

Branching ratios are admixtures of charm and bottom hadrons

$$\begin{aligned} B(D \to e) &= 10.3 \pm 1.2\,\% \\ B(B \to e) &= 10.86 \pm 0.35\,\% \\ B(B \to D \to e) &= 9.6 \pm 0.6\,\% \end{aligned}$$

Work in progress with M. Djordjevic to study energy loss effects on single electrons from heavy flavor decays

Uncertainty Bands for Electrons from Heavy Flavor Decays at 200 GeV

Electrons from B decays begin to dominate at $p_T \sim 5$ GeV

Electron spectra very sensitive to rapidity range – to get $|y| \leq 0.75$ electrons, need $|y| \leq 2$ charm and bottom range

Forward electron spectra thus not possible to obtain using FONLL code due to problems at large y

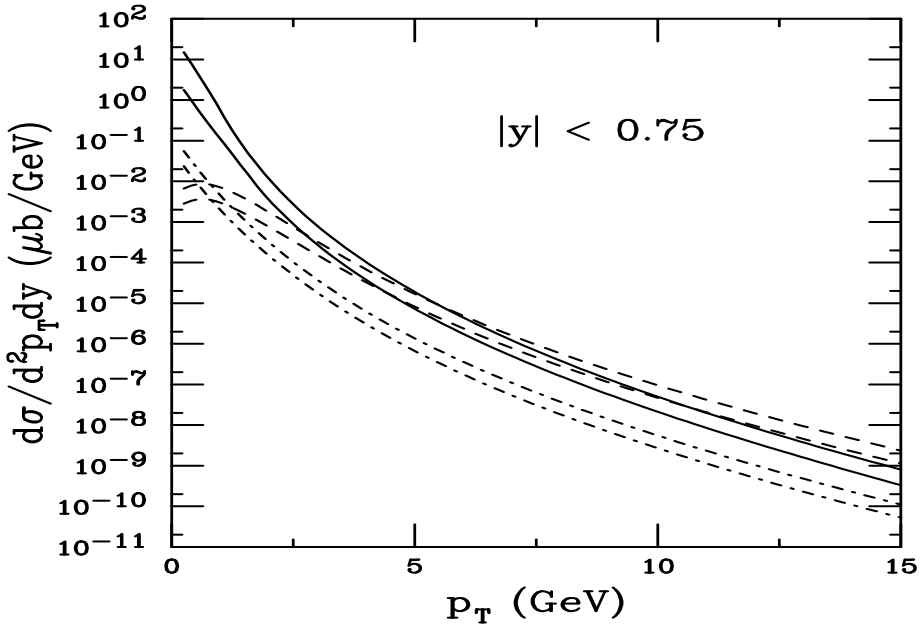

Figure 7: The theoretical FONLL bands for $D \to eX$ (solid), $B \to eX$ (dashed) and $B \to DX \to eX'$ (dot-dashed) as a function of p_T in $\sqrt{s} = 500$ GeV pp collisions for $|y| < 0.75$.

Comparison to Electron Data at 200 GeV

Includes PHENIX preliminary data from *pp* and STAR published and preliminary data

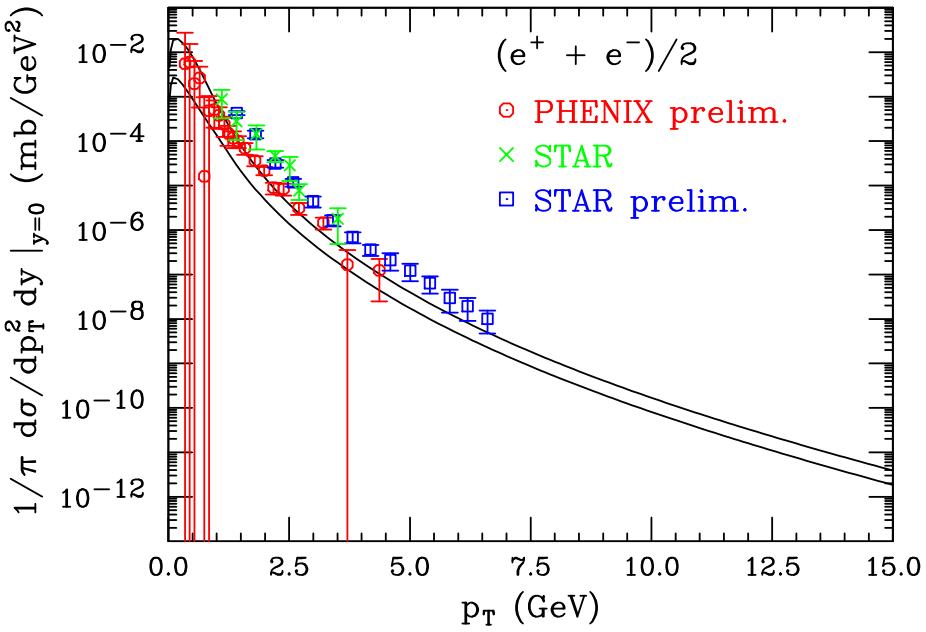

Figure 8: Prediction of the theoretical uncertainty band of the total electron spectrum from charm and bottom (Cacciari, Nason and RV). Preliminary data from PHENIX and STAR are also shown.

Uncertainty Bands for Electrons from Heavy Flavor Decays at 500 GeV

Crossover between B and D dominance is similar at the higher energy

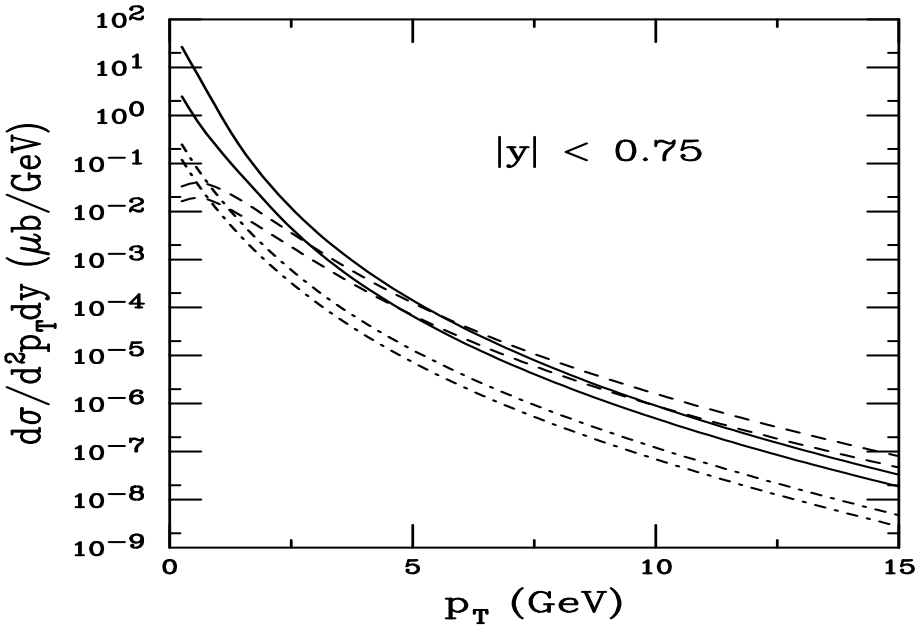

Figure 9: The theoretical FONLL bands for $D \to eX$ (solid), $B \to eX$ (dashed) and $B \to DX \to eX'$ (dot-dashed) as a function of p_T in $\sqrt{s} = 500$ GeV pp collisions for $|y| < 0.75$.

Comparison of Components of $D \to e$ and $B \to e$ Bands at 200 GeV

Comparison done in the crossover region $3 < p_T < 10$ GeV

Here $(\mu_F/m_T, \mu_R/m_T) = (0.5, 0.5)$ and (2,2) bracket the band from above and below — mass uncertainty is larger than scale uncertainty

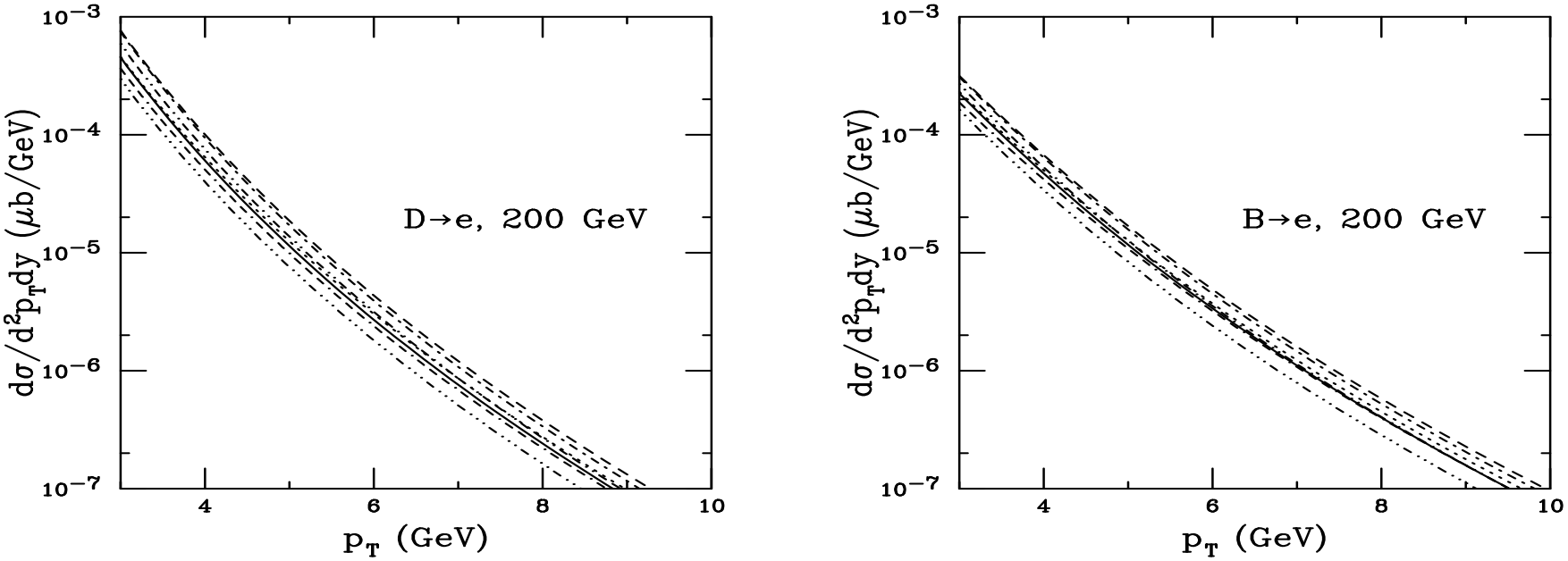

Figure 10: The solid curve is the central value $(\mu_F/m_T, \mu_R/m_T) = (1, 1)$ with $m = 1.5$ (charm) and 4.75 GeV (bottom). The upper and lower dashed curves are the lower and upper mass values with (1,1) respectively. The upper and lower dot-dashed curves correspond to (0.5,0.5) and (2,2) while the upper and lower dotted curves are with (1,0.5) and (0.5,1) and the upper and lower dot-dot-dot-dashed curves are with (2,1) and (1,2) with the central mass value for $\sqrt{s} = 200$ GeV pp collisions for $|y| < 0.75$.

Comparison of Components of $D \to e$ and $B \to e$ Bands at 500 GeV

Similar behavior as at the lower energy

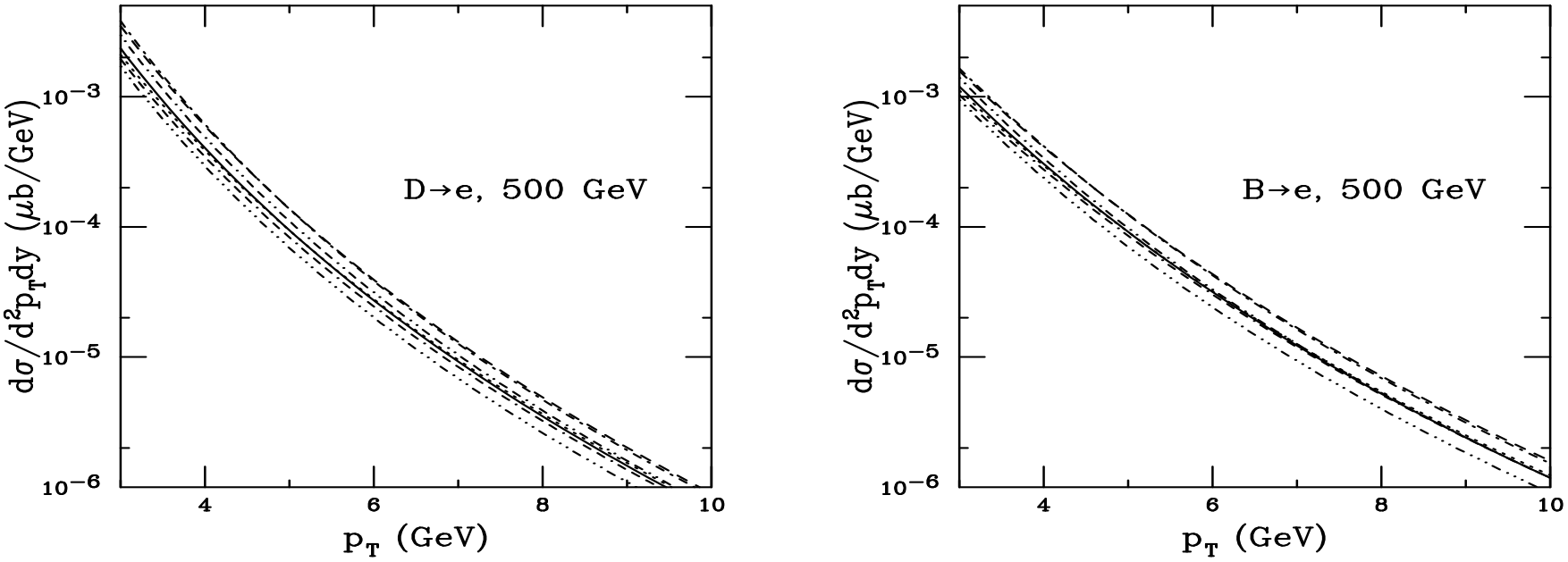

Figure 11: The solid curve is the central value $(\mu_F/m_T, \mu_R/m_T) = (1, 1)$ with $m = 1.5$ (charm) and 4.75 GeV (bottom). The upper and lower dashed curves are the lower and upper mass values with (1,1) respectively. The upper and lower dot-dashed curves correspond to (0.5,0.5) and (2,2) while the upper and lower dotted curves are with (1,0.5) and (0.5,1) and the upper and lower dot-dot-dot-dashed curves are with (2,1) and (1,2) with the central mass value for $\sqrt{s} = 200$ GeV pp collisions for $|y| < 0.75$.

Drell-Yan Production at RHIC

Lepton Pair Production to NLO

Production of a lepton pair with mass M at scale μ at next-to-leading order

$$\frac{1}{AB}\frac{d\sigma_{AB}}{dMdy} = \int dx_1 dx_2 dx \delta\Big(\frac{M^2}{s} - x x_1 x_2\Big)\delta\Big(y - \frac{1}{2}\ln\Big(\frac{x_1}{x_2}\Big)\Big)\Big\{\sum_{i,j\in Q,\overline{Q}} H_{ij} C^{\rm ii}(q_i,\overline{q}_j)\Delta_{q\overline{q}}(x) F^A_{q_i}(x_1,\mu^2) F^B_{\overline{q}_j}(x_2,\mu^2)$$
$$+ \sum_{i,k\in Q,\overline{Q}} H_{ij} C^{\rm if}(q_i,q_k)\Delta_{qg}(x)\Big[F^A_{q_i}(x_1,\mu^2)F^B_g(x_2,\mu^2) + F^A_g(x_1,\mu^2)F^B_{q_j}(x_2,\mu^2)\Big]\Big\}$$

There are three contributions to continuum lepton pair production: virtual photon exchange, Z^0 exchange, and $\gamma* - Z^0$ interference – virtual photon exchange dominant at small M (≤ 20 GeV) and intermediate energies (like RHIC)

$$\begin{aligned}
H_{ij} &= H^{\gamma*}_{ij} + H^{\gamma*-Z^0}_{ij} + H^{Z^0}_{ij} \\
H^{\gamma*}_{ij} &= \frac{4\pi\alpha^2}{9M^2 s}|e_i|^2 \\
H^{\gamma*-Z^0}_{ij} &= \frac{\alpha}{9}\frac{G_F}{\sqrt{2}}\frac{m_Z^2}{s}\frac{(1-4\sin^2\theta_W)(M^2-m_Z^2)}{(M^2-m_Z^2)^2+m_Z^2\Gamma_Z^2}|e_i|(1-4|e_i|\sin^2\theta_W) \\
H^{Z^0}_{ij} &= \frac{1}{3}\frac{G_F}{\sqrt{2}}\frac{M^2}{s}\frac{m_Z\Gamma_{Z\to l^+l^-}}{(M^2-m_Z^2)^2+m_Z^2\Gamma_Z^2}(1+(1-4|e_i|\sin^2\theta_W)^2) \\
\Gamma_{Z\to l^+l^-} &= \frac{\alpha m_Z(1+(1-4\sin^2\theta_W)^2)}{48\sin^2\theta_W\cos^2\theta_W} \\
\Gamma_Z &= 2.492 \text{ GeV}
\end{aligned}$$

We use CTEQ6M and with $\mu = M$

Universal Corrections to the LO Drell-Yan Cross Section

.

$$\Delta_{q\bar{q}}(x) = \delta(1-x) + \frac{\alpha_s}{3\pi}\Big\{ -4(1+x)\ln\Big(\frac{\mu^2}{M^2}\Big) - 8(1+x)\ln(1-x) - 4\frac{1+x^2}{1-x}\ln x$$
$$+ \delta(1-x)\Big[6\ln\Big(\frac{\mu^2}{M^2}\Big) + 8\zeta(2) - 16\Big] + 8\mathcal{D}_0(x)\ln\Big(\frac{\mu^2}{M^2}\Big) + 16\mathcal{D}_1(x)\Big\} .$$

$$\mathcal{D}_i(x) = \delta(1-x)\frac{\ln^{i+1}}{i+1} + \theta(1-\delta-x)\frac{\ln^i(1-x)}{1-x}$$

$$\int_a^1 dx f(x)\Big[\frac{\ln(1-x)}{1-x}\Big]_+ = \int_a^1 dx \frac{f(x)-f(1)}{1-x}\ln(1-x) + \frac{1}{2}f(1)\ln^2(1-x)$$

$$\Delta_{qg}(x) = \frac{\alpha_s}{8\pi}\Big\{2(1+2x^2-2x)\ln\Big(\frac{(1-x)^2\mu^2}{xM^2}\Big) + 1 - 7x^2 + 6x\Big\} .$$

$(g_V^i)^2 + (g_A^i)^2 = (1/8)(1 - 4|e_i|x_W + 8e_i^2 x_W^2)$
where $x_W = \sin^2\theta_W = 1 - m_W^2/m_Z^2$

Dilepton Production: Convolution of Shadowing Functions with Parton Densities

$$\sum_{i,j\in Q\overline{Q}} S^i(A,x_1)S^j(B,x_2)f_{q_i}^N(x_1,Q^2)f_{\overline{q}_j}^N(x_2,Q^2)C^{\rm ii}(q_i,\overline{q}_j)H_{ij}$$

$$= H_{uu}\left(S^u(A,x_1)S^{\overline{u}}(B,x_2)\left\{Z_A f_u^p(x_1,Q^2)+N_A f_u^n(x_1,Q^2)\right\}\right.$$
$$\times\left\{Z_B f_{\overline{u}}^p(x_2,Q^2)+N_B f_{\overline{u}}^n(x_2,Q^2)\right\}+2ABS^c(A,x_1)S^{\overline{c}}(B,x_2)f_c^p(x_1,Q^2)f_{\overline{c}}^p(x_2,Q^2)\Big)$$
$$+H_{dd}\left(S^d(A,x_1)S^{\overline{d}}(B,x_2)\left\{Z_A f_d^p(x_1,Q^2)+N_A f_d^n(x_1,Q^2)\right\}\right.$$
$$\times\left\{Z_B f_{\overline{d}}^p(x_2,Q^2)+N_B f_{\overline{d}}^n(x_2,Q^2)\right\}+2ABS^s(A,x_1)S^{\overline{s}}(B,x_2)f_s^p(x_1,Q^2)f_{\overline{s}}^p(x_2,Q^2)\Big)$$
$$+[x_1\leftrightarrow x_2, A\leftrightarrow B]\ .$$

$$\sum_{i,k\in Q\overline{Q}}\Big(S^i(A,x_1)S^g(B,x_2)f_{q_i}^N(x_1,Q^2)f_g^N(x_2,Q^2)+[x_1\leftrightarrow x_2,A\leftrightarrow B]\Big)C^{\rm if}(q_i,q_k)H_{ij}$$

$$= BS^g(B,x_2)f_g^p(x_2,Q^2)\times\Big\{H_{uu}\left(S^u(A,x_1)\left\{Z_A f_u^p(x_1,Q^2)+N_A f_u^n(x_1,Q^2)\right\}\right.$$
$$+S^{\overline{u}}(A,x_1)\left\{Z_B f_{\overline{u}}^p(x_2,Q^2)+N_B f_{\overline{u}}^n(x_2,Q^2)\right\}+2AS^c(A,x_1)f_c^p(x_1,Q^2)\Big)$$
$$+H_{dd}\left(S^d(A,x_1)\left\{Z_A f_d^p(x_1,Q^2)+N_A f_d^n(x_1,Q^2)\right\}\right.$$
$$+\left.\left.S^{\overline{d}}(A,x_1)\left\{Z_B f_{\overline{d}}^p(x_2,Q^2)+N_B f_{\overline{d}}^n(x_2,Q^2)\right\}+2AS^s(A,x_1)f_s^p(x_1,Q^2)\right)\right\}$$
$$+[x_1\leftrightarrow x_2,A\leftrightarrow B]\ .$$

Comparing Shadowing Parameterizations: x Dependence

Recent parameterizations by Frankfurt *et al* (FGSo, FGSh, FGSl) EKS98 for valence shadowing, stronger gluon shadowing at low x, cuts off modification above $x = 0.25$ for sea, 0.03 for gluon

Newer FGS parameterizations (FGSh and FGSl) have lower gluon antishadowing, smoother x dependence over $10^{-4} < x < 0.02$ – and identical sea quark shadowing

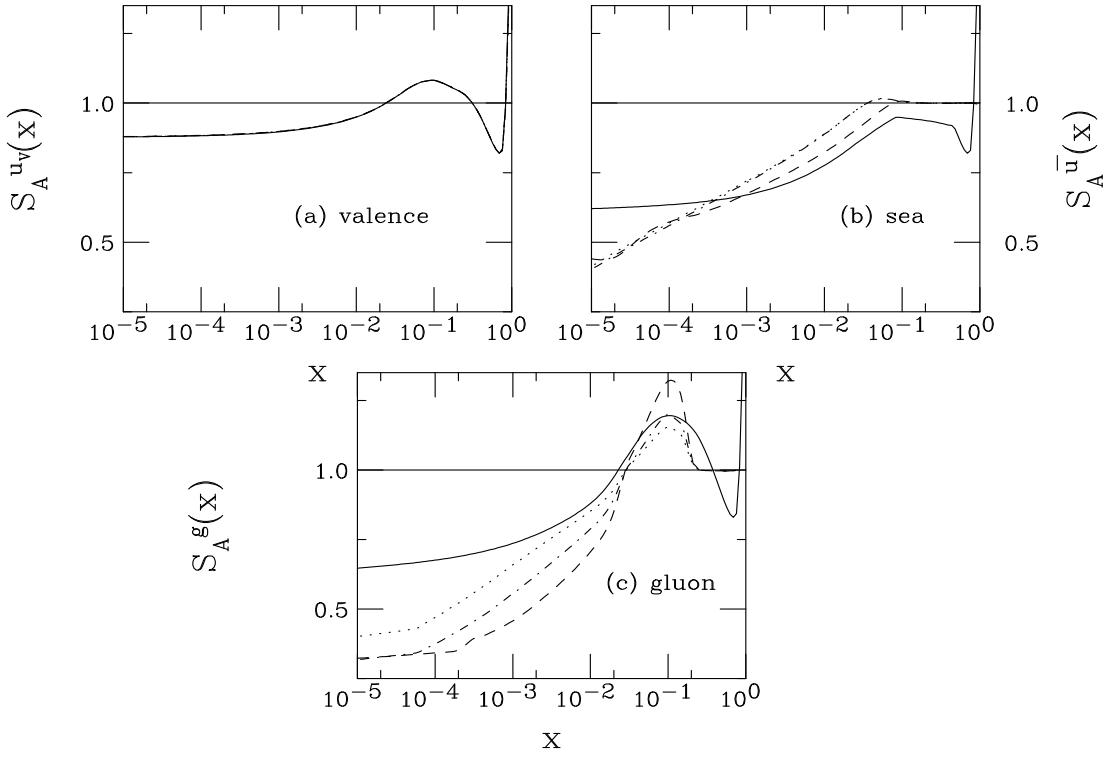

Figure 12: The EKS98 and FGS shadowing parameterizations are compared at the scale $\mu = 2m = 2.4$ GeV. The solid curves are the EKS98 parameterization, the dashed, FGSo, dot-dashed, FGSh, dotted, FGSl.

Drell-Yan Mass Distributions in 200 GeV pp and d+Au Collisions

Main difference between pp and d+Au slopes at forward and backward rapidity is due to isospin, shadowing seen at low M, largest for $1.2 < y < 2.2$

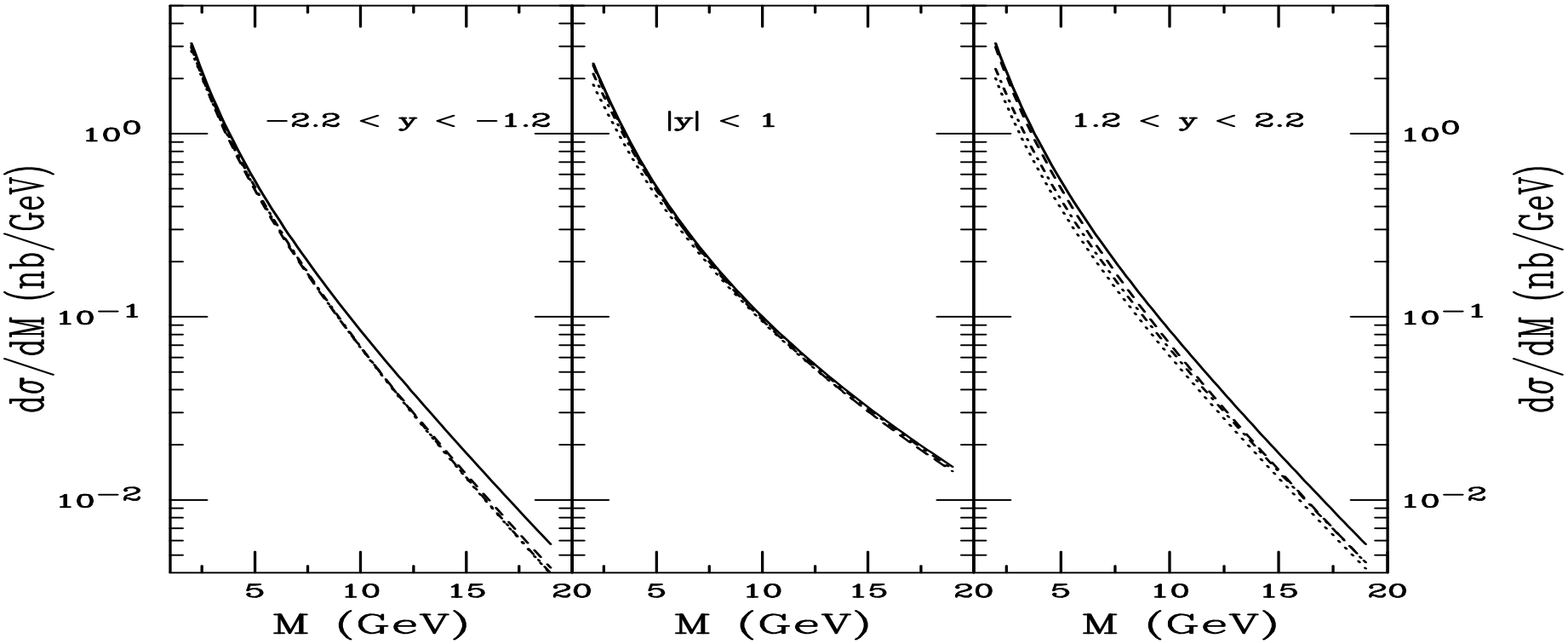

Figure 13: The dilepton mass distributions in pp and d+Au collisions at 200 GeV in the rapidity windows: $-2.2 < y < -1.2$ (left); $|y| < 1$ (center); and $1.2 < y < 2.2$ (right). The solid curve is the pp distribution while the dashed, dot-dashed and dotted curves are the d+Au results without shadowing, with FGSh and EKS98 shadowing parameterizations respectively.

Shadowing Effects on Drell-Yan Mass Distributions

Little difference between parameterizations in backward region due to same valence shadowing in both cases, effect increases with rapidity and decreases with mass

Effect largest for EKS98 with stronger sea quark shadowing for $x > 0.001$

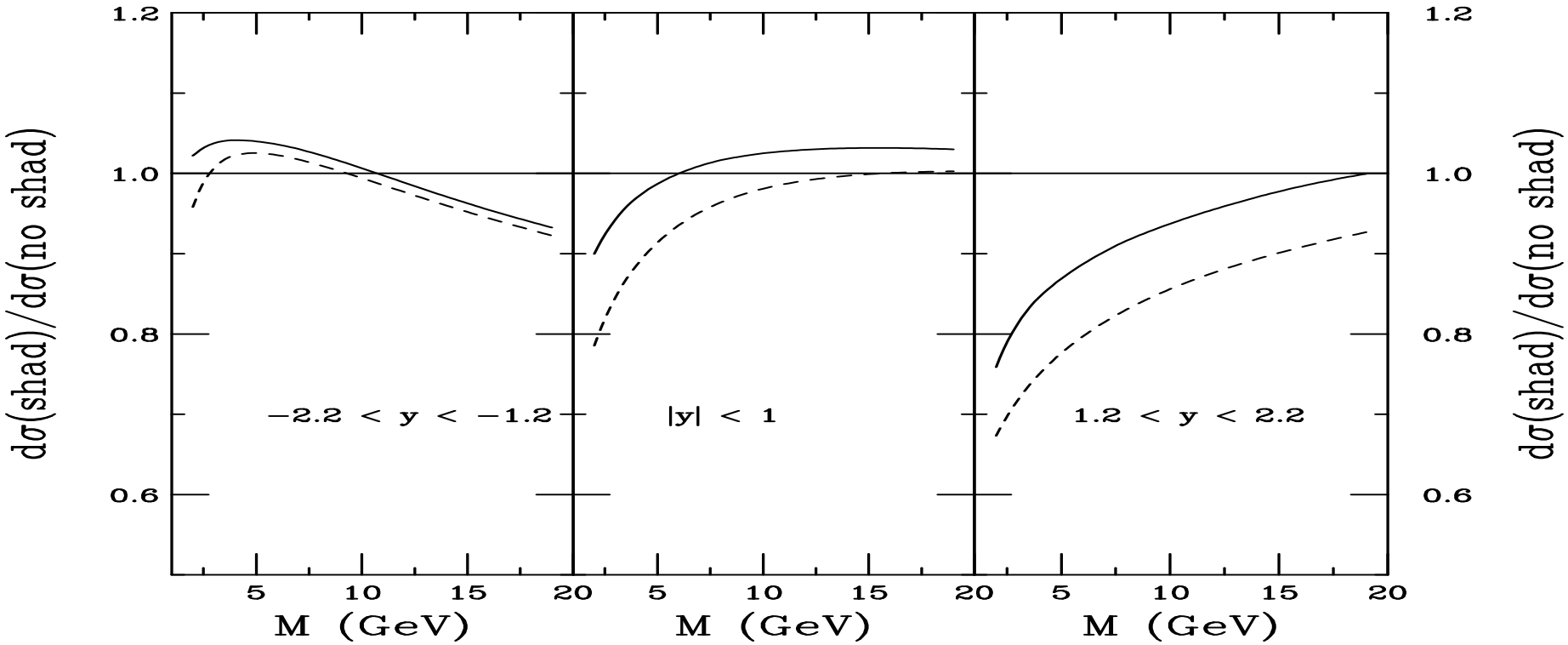

Figure 14: The dilepton shadowing ratios in d+Au collisions at 200 GeV in the rapidity windows: $-2.2 < y < -1.2$ (left); $|y| < 1$ (center); and $1.2 < y < 2.2$ (right). The solid curve is the FGSh ratio while the dashed curve is the EKS98 result.

Drell-Yan Mass Distributions in 500 GeV pp Collisions

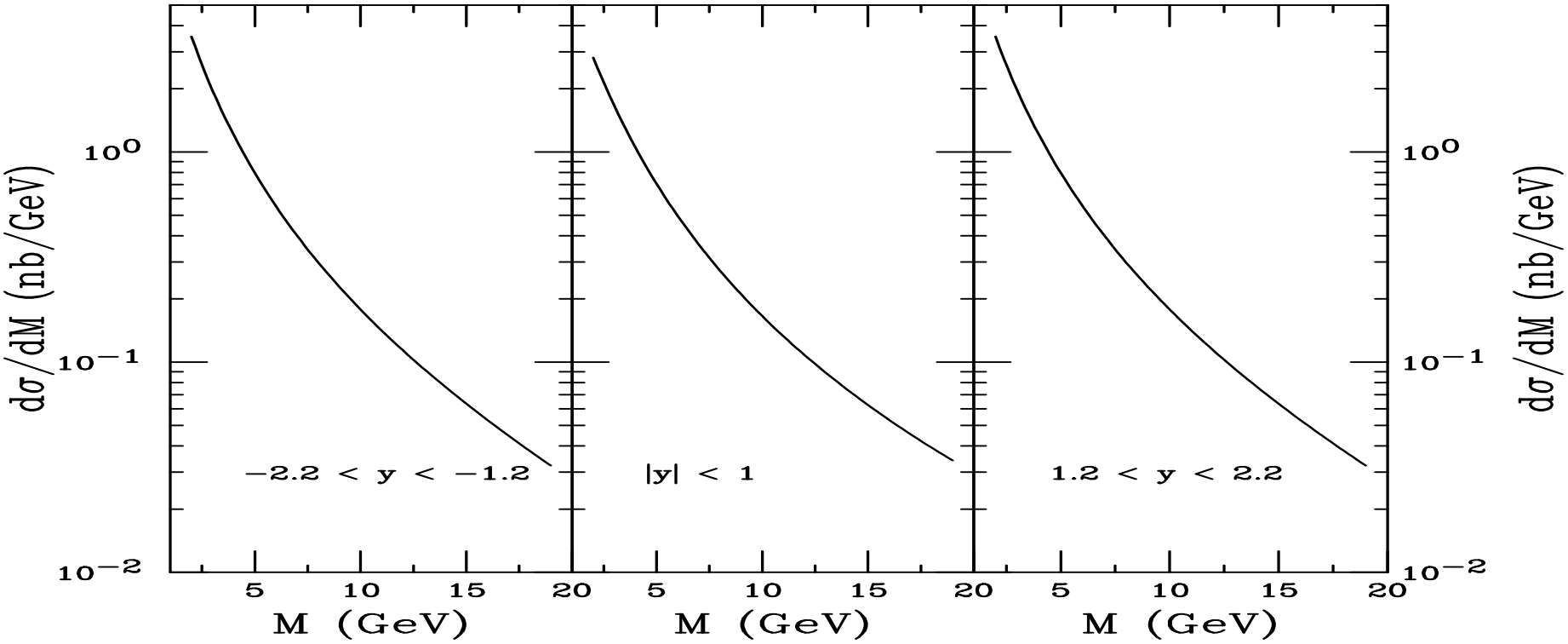

Figure 15: The dilepton mass distributions in pp collisions at 500 GeV in the rapidity windows: $-2.2 < y < -1.2$ (left); $|y| < 1$ (center); and $1.2 < y < 2.2$ (right).

Dependence of K Factors on Mass in 200 and 500 GeV pp Collisions

K factors largest for low masses, lower energy

Increase with mass, especially away from midrapidity, due to approach of edge of phase space

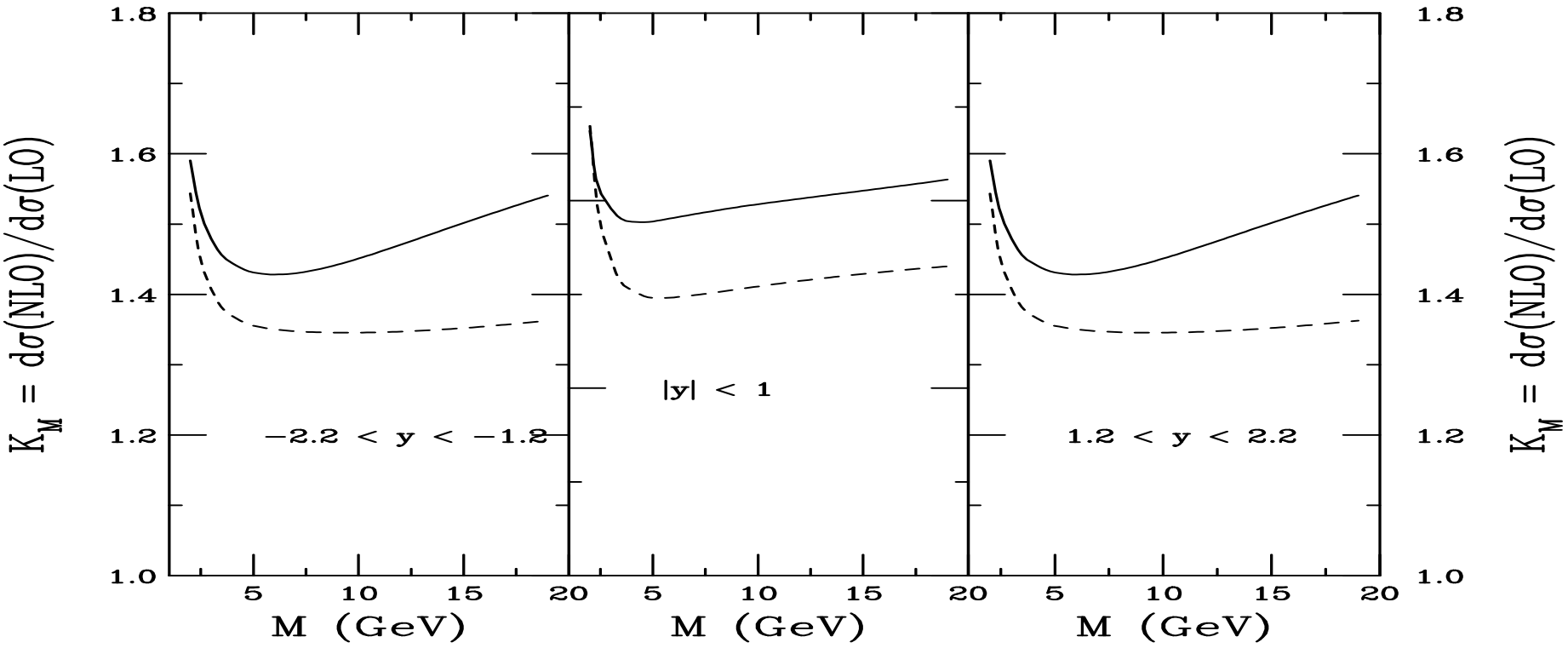

Figure 16: The dilepton K factors as a function of mass in pp collisions at 200 and 500 GeV in the rapidity windows: $-2.2 < y < -1.2$ (left); $|y| < 1$ (center); and $1.2 < y < 2.2$ (right). The solid curves are for 200 GeV while the dashed curves are for 500 GeV.

Drell-Yan Rapidity Distributions in 200 GeV pp and d+Au Collisions

Rapidity distributions increase away from midrapidity due to behavior of low x parton densities at low masses, not seen for largest mass bin

pp curves symmetric, asymmetry due to shadowing

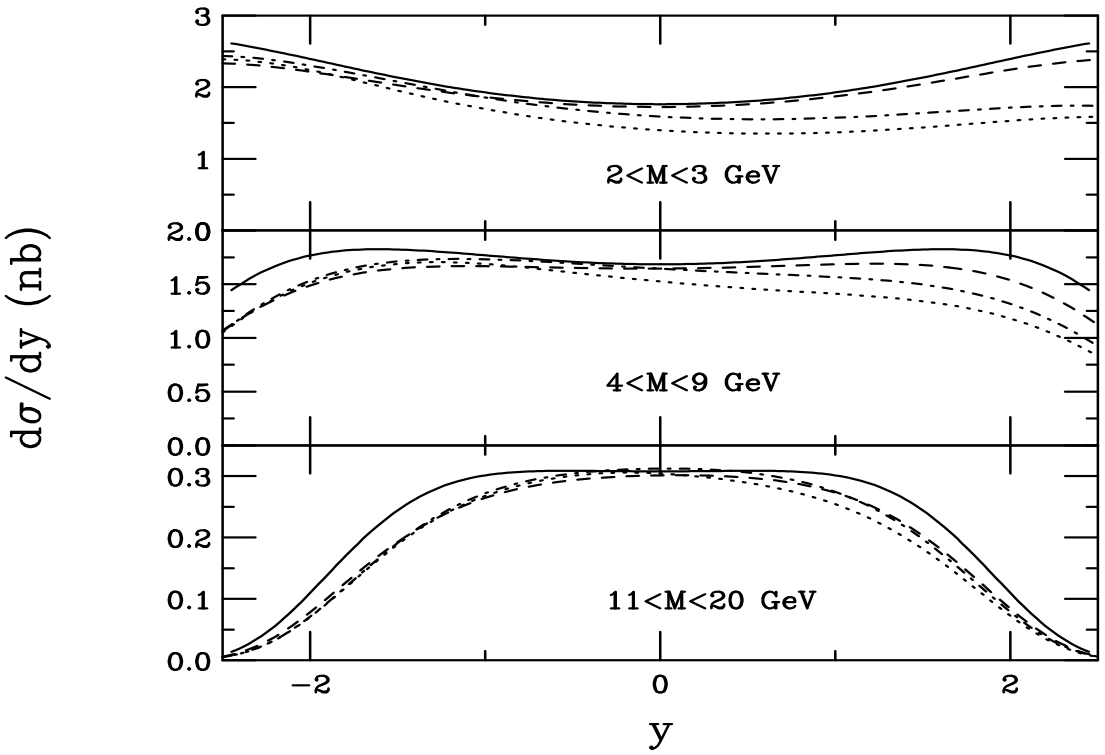

Figure 17: The dilepton rapidity distributions in pp and d+Au collisions at 200 GeV in the mass windows: $2 < M < 3$ GeV (top); $4 < M < 9$ GeV (center); and $11 < M < 20$ GeV (bottom). The solid curve is the pp distribution while the dashed, dot-dashed and dotted curves are the d+Au results without shadowing, with FGSh and EKS98 shadowing parameterizations respectively.

Shadowing Effects on Drell-Yan Rapidity Distributions

Some evidence of antishadowing and EMC (same for both due to identical valence shadowing) behavior at negative rapidities with shadowing apparent (especially for low masses) at forward rapidity

EKS98 effect of sea quark shadowing stronger

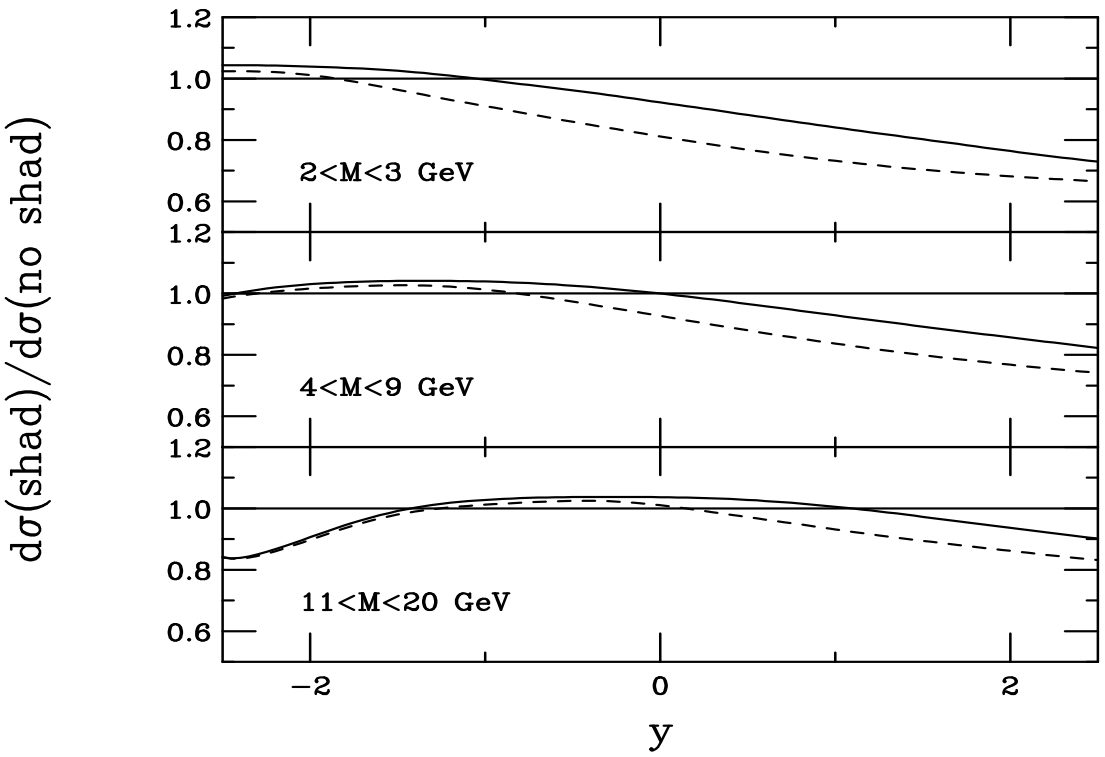

Figure 18: The dilepton shadowing ratios in d+Au collisions at 200 GeV in the mass windows: $2 < M < 3$ GeV (top); $4 < M < 9$ GeV (center); and $11 < M < 20$ GeV (bottom). The solid curve is the FGSh ratio while the dashed curve is the EKS98 result.

Drell-Yan Rapidity Distributions in 500 GeV pp Collisions

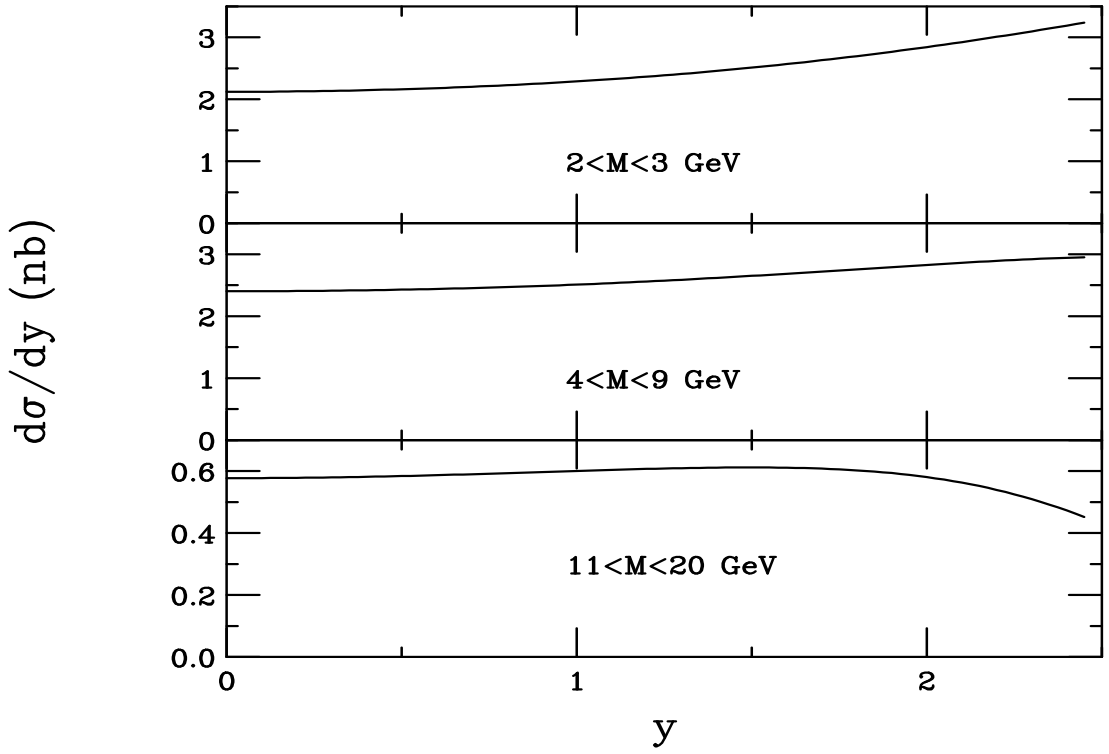

Figure 19: The dilepton rapidity distributions in pp collisions at 500 GeV in the mass windows: $2 < M < 3$ GeV (top); $4 < M < 9$ GeV (center); and $11 < M < 20$ GeV (bottom).

Dependence of K Factors on Rapidity in 200 and 500 GeV pp Collisions

K factors fairly constant with y

Only $y > 0$ shown because K is symmetric around $y = 0$

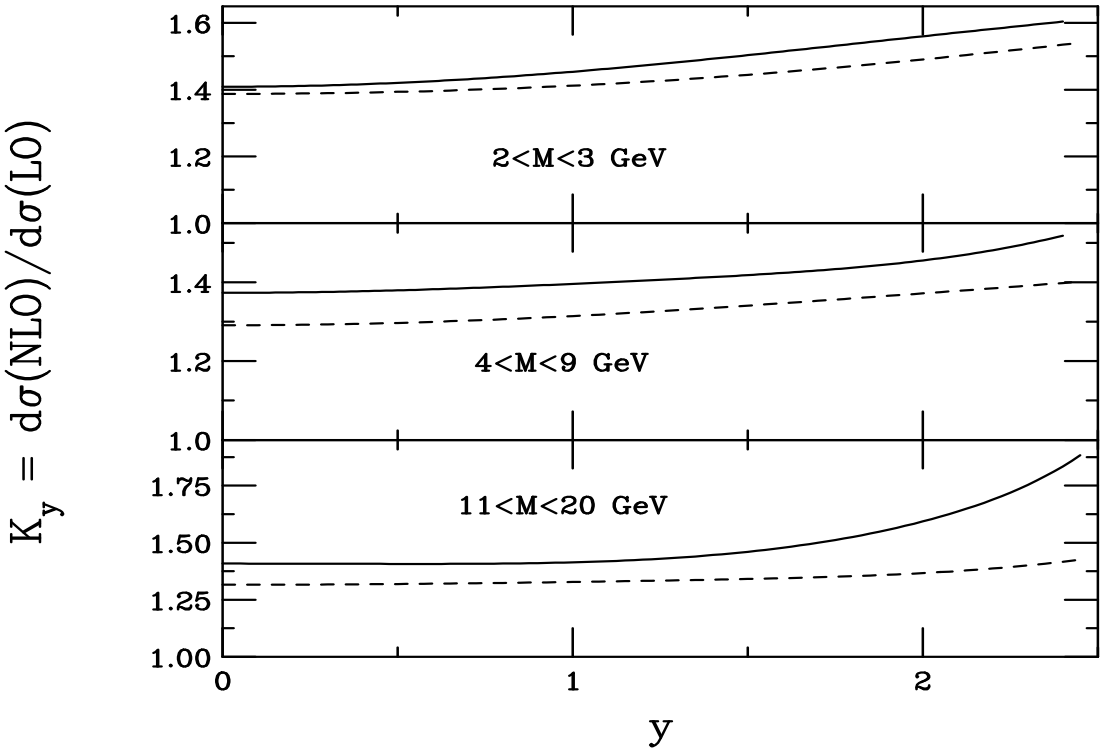

Figure 20: The dilepton K factors as a function of y in pp collisions at 200 and 500 GeV in the mass windows: $2 < M < 3$ GeV (top); $4 < M < 9$ GeV (center); and $11 < M < 20$ GeV (bottom). The solid curves are for 200 GeV while the dashed curves are for 500 GeV.

Summary .

- Contributions of D and B decays to leptons difficult to disentangle and would require precision measurements of their decays to hadrons to better distinguish
- Drell-Yan cross sections at low mass exhibit quark shadowing – gluon contribution to total is not so large since K factors also include NLO $q\overline{q} \to g\gamma^*$